RESEARCH ARTICLE

VOLCANICA

Fe-rich filamentary textures reveal timescales of magmatic interaction before the onset of high-energy explosive events at basaltic volcanoes

Claudia D'Oriano*[α], Chiara P. Montagna[α], Simone Colucci[α], Paola Del Carlo[α], Federico Brogi[α], Daniele Morgavi[β], Alessandro Musu[γ], Fabio Arzilli[δ], Simone Costa[α], and Patrizia Landi[α]

[α]Istituto Nazionale di Geofisica e Vulcanologia, Sezione di Pisa, Via Cesare Battisti 53, 56125 Pisa, Italy.
[β]Dipartimento di Scienze della Terra, dell'Ambiente e delle Risorse, Università degli Studi di Napoli Federico II, via Cintia, 21, 80126 Napoli, Italy.
[γ]Department of Lithospheric Research, University of Vienna, UZA2, Josef-Holaubek-Platz 2, 1090 Vienna, Austria.
[δ]School of Science and Technology, Geology Division, University of Camerino, Via Gentile III da Varano, 7, 62032 Camerino, Italy.

Abstract

Fe-rich filamentary textures are almost ubiquitous in products from explosive eruptions at basaltic volcanoes and, in particular, they characterize the groundmass of ash and lapilli emitted during high-energy events. Here, we present a multidisciplinary study integrating petrological analyses with computational fluid dynamics simulations to propose a new mechanism responsible for their formation. Detailed textural and compositional features of Fe-rich filaments were examined in the products of explosive eruptions with different intensities from Stromboli and Etna (Italy) volcanoes. Results reveal that they represent compositional boundary layers developed at the plagioclase-melt interface in response to the interaction between magmas with different compositions and volatile contents. Numerical simulations indicate that boundary layers can detach from crystals and disperse into resident melts due to their higher density and can survive as metastable melts for some days under magmatic conditions. We suggest that Fe-rich filaments testify to the recharging of deep magma a few days before high-energy explosive events at basaltic open-vent volcanoes, even when primitive magmas are not erupted.

Riassunto

Filamenti ricchi in Fe sono presenti in quasi tutti i prodotti di eruzioni esplosive in vulcani basaltici e, in particolare, caratterizzano la massa di fondo di cenere e lapilli emessi durante eventi ad alta energia. In questo articolo presentiamo uno studio multidisciplinare che integra analisi petrologiche con simulazioni di fluidodinamica computazionale per proporre un nuovo meccanismo responsabile della loro formazione. Le caratteristiche tessiturali e composizionali dei filamenti ricchi in Fe sono state esaminate nel dettaglio in prodotti di eruzioni esplosive a diversa intensità avvenute sia a Stromboli che all'Etna (Italia). I risultati suggeriscono che essi rappresentino le interfacce composizionali tra i cristalli di plagioclasio e il liquido circostante che si sviluppano in seguito all'interazione tra magmi con diversa composizione e contenuto in volatili. Le simulazioni numeriche hanno evidenziato che tali interfacce composizionali si possono staccare dai cristalli e disperdersi nei liquidi circostanti a causa della loro alta densità e possono sopravvivere come liquidi metastabili per alcuni giorni alle condizioni magmatiche. Si ipotizza che i filamenti ricchi di Fe siano la testimonianza di una ricarica di magma profondo che avviene pochi giorni prima di eventi esplosivi ad alta energia in vulcani basaltici a condotto aperto, anche quando i magmi primitivi non vengono eruttati.

Keywords: Basaltic volcanoes; Fe-rich melts; Micro-textures; Geochemistry; Magmas interaction; Timescales.

1 Introduction

Basaltic volcanoes are among the most spectacular and accessible outdoor adventure attractions [Wadsworth et al. 2022], and a large number of people live along their flanks as they have the reputation of being "good volcanoes". Nevertheless, they are characterized by sudden transitions in eruptive styles that drastically increase the associated risk [Vergniolle and Métrich 2022].

At some basaltic, open-conduit volcanoes (i.e. Etna and Stromboli in Italy; Villarrica in Southern Chile), the shift toward more energetic events has been associated with the arrival of CO_2-rich fluids in the shallow systems days/weeks before the paroxysms [Aiuppa et al. 2017; 2021; Caricchi et al. 2024], sourced by the intrusion of hotter and primitive, volatile-rich magma [Andronico et al. 2021; Romero et al. 2022]. Processes occurring from the time of intrusion to a possible high-energy event encompass magma degassing, crystallization, mixing, and variable interaction with the crystal mush. Petrological evidence of these processes is usually captured by the composition of mineral phases, and specifically by their zoning patterns and elemental diffusion profiles. However, they are rarely identified in the composition and texture of residual glasses, which better record the last input of the deep recharge that triggers the eruption [Morgavi et al. 2017, and references therein].

In the products emitted at Stromboli and Etna before and during high-energy explosive events, we found abundant Fe-rich filamentary textures, not present in the products emitted during ordinary activity. Similar textures have been previously observed in the groundmass from basaltic volcanoes, both as natural and experimental products.

*claudia.doriano@ingv.it

Submitted: 2024-09-03 | Accepted: 2025-02-06 | Published: 2025-03-27

Editor: F. Wadsworth | Typesetter: J. Farquharson

Laumonier et al. [2014] detected Fe-rich melts in mixing experiments between mafic and felsic magmas conducted at high temperature (1170–1200 °C) and high pressure (300 MPa). In these experiments, crystal-free melt layer formed at the interaction zone between the two magmas during long experiments, lasting 50 hours under static conditions. Filaments, showing heterogeneous chemical composition characterized by high FeO, CaO, and MgO contents, were associated with remnants of these melt pockets stretched under torsional experiments.

During the recent 2021 Tajogaite eruption of Cumbre Vieja (Canary Islands, Spain), Fe-rich filamentary textures have been described within the matrix glasses of products emitted during the first phase (first week) of the eruption. They were correlated with the ascent of primitive basanitic melts from a deep storage level of 25–35 km, dragged by gas bubbles, which induced an increase in the explosive behaviour of the basaltic magma [González-García et al. 2023]. The preservation timing of these filaments has been estimated to be in the order of seconds to a minute, allowing to associate them with the latest phase of magma ascent from the sub-Moho depths.

Moving toward the shallower portions of a volcano plumbing system, in a study focused on a large dataset of products emitted at basaltic volcanoes during explosive events, Fe-rich filamentary textures were interpreted as partial healing of brittle fractures propagated within the magma column in the upper conduit before melt quenching/ eruption [Taddeucci et al. 2021].

The Fe-rich textures present in samples from Stromboli and Etna can only be partially interpreted with the mechanisms proposed in the literature, which consider a wide range of magmatic conditions and timescales. To find a possible mechanism responsible for the formation of Fe-rich filaments at Stromboli and reconcile it with previous works, we integrated chemical and textural analyses with computational fluid dynamics simulations. The same information was collected on pyroclasts from Etna, giving interesting results that allow us to extend the new insights to basaltic volcanoes in general.

1.1 Stromboli eruptive styles and magma composition

Stromboli is considered as a case study for basaltic explosive eruptions due to its frequent activity, ranging from the iconic and persistent "normal" Strombolian explosions to more energetic events with variable intensity, named "major explosions" and "paroxysms" [Rosi et al. 2013]. During "normal activity," a shallow, highly-porphyritic (HP) magma, characterized by a shoshonitic glass composition, with ~50 vol.% of crystals (mainly plagioclase), is erupted. The rare "paroxysms" (0.1 events/year [Bevilacqua et al. 2020]) interrupt this behaviour, triggered by the arrival of a hotter, volatile-rich, low-porphyritic (LP) magma, with a shoshonitic basaltic glass composition and less than 10 vol.% of crystals (olivine and pyroxene), ascending from 6–9 km deep [Métrich et al. 2021]. "Major explosions," intermediate explosive events with a spectrum of intensities ranging between normal activity and paroxysms [Ripepe et al. 2021], occur with a frequency of ~3 events/year [Pioli et al. 2014; Bevilacqua et al. 2020]. The triggering of major explosions at Stromboli has also been linked to the ascent of LP magma, although not all major explosions are associated with the emission of LP magma [Métrich et al. 2001]. Petrological studies indicate that, in products from major explosions, processes acting at intermediate depths (<100 MPa), where the LP magma crystallizes, degasses, and mixes with the resident HP magma, are recorded by the textural and chemical features of groundmass glass and mineral phases [Landi et al. 2004; La Felice and Landi 2011; Pioli et al. 2014; Métrich et al. 2021; Landi et al. 2022; Pichavant et al. 2022; Voloschina et al. 2023].

2 Samples and Methods

Studied samples were collected during the April–June 2022 field surveys on the volcano summit area Pizzo Sopra La Fossa. They consist of juvenile fragments emitted during "normal activity" on 11 April (lapilli) and 29 June 2022 (coarse ash) and the "major explosion" which occurred on 13 May 2022 (lapilli). We also analysed lapilli from the major explosions of 8 and 24 November 2009 [La Felice and Landi 2011], 19 July 2020 [Landi et al. 2022; Voloschina et al. 2023], and 6 October 2021 [Landi et al. 2022]; and lapilli from the 3 July and coarse ash from the 28 August 2019 paroxysms [Andronico et al. 2021]. These samples represent the whole spectrum of compositions emitted at Stromboli, from HP scoriae to mingled HP and LP products to LP pumices [Bertagnini et al. 2008]. In addition, we analysed also samples from Etna: coarse ash from the 23–24 March 2021 lava fountain [Andronico et al. 2024]; lapilli from the powerful Strombolian-like explosion of 24 December 2018 [Laiolo et al. 2019]; and fine ash from the following ash-rich emission of 23 January 2019 that started the January-February 2019 ash-emission cycle [D'Oriano et al. 2022].

2.1 Textural and compositional characteristics

Ash and lapilli were glued in epoxy resin and polished to 1 µm with alumina grit paste in order to expose their internal portions. The resulting 1-inch mounts were carbon-coated for SEM inspection. We selected three lapilli from each sample and for each lapillus we analysed a portion of approximately 1 cm^2. Backscattered scanning electron microscope (SEM-BSE) images and preliminary major element chemical composition of matrix glass were acquired at INGV-Pisa using a Zeiss EVO MA 10 SEM, equipped with an Oxford ISIS microanalytical EDS system. Quantitative SEM-EDS chemical analyses were obtained via standard calibration, and the accuracy of the results was checked against repeated analyses of the reference basaltic glass VG2 (Supplementary Material 1 Table S1). The detailed methodology, standard, and errors related to SEM-EDS analyses of glasses are the same as those presented in D'Oriano et al. [2022].

For each sample, 3–4 chemical maps of the glass matrix were acquired, for a total of 15 maps, each with an area of approximately 0.22 mm^2 (±0.08 mm^2). High-resolution chemical maps were acquired using a JEOL JXA-8530F field-emission electron probe microanalyser (FE-EPMA) installed at University of Cambridge (UNICAM). For beam calibration, natural and synthetic crystals were used as follows: SiO_2 for Si, TiO_2 for Ti, Al_2O_3 for Al, Fe_2O_3 for Fe, MnO for Mn, MgO for Mg, wollastonite for Ca, jadeite for Na, K-feldspar for K,

halite for Cl, and $BaSO_4$ for S. The Cl count was measured using a PETH crystal, which enabled higher count rates compared to those obtained with a traditional PET crystal. The acceleration voltage and probe current were 15 kV and 10–100 nA, respectively. The highest beam current is used to obtain a higher count rate for Cl [Yoshimura et al. 2019]. The beam diameter was 2 µm. The mapping analysis was conducted by moving the stage by 2 µm along the x and y directions at each step. Dwell time at each step was 500 ms. Compositional profiles across zones between melts with different elemental concentration were realized both at UNICAM with the JEOL JXA-8530F FE-EPMA and INGV-Rome, with a Jeol-JXA8200 combined EDS-WDS (five spectrometers with twelve crystals). The acceleration voltage and beam current were 15 kV and 10 nA, respectively. A ZAF correction method was applied to all analyses. The beam diameter was 2 µm. Analyses reproducibility was checked against repeated measures of VG-A99 (UNICAM) and BCR-2 (INGV-Rome) basaltic reference glasses, resulting in an error <5 % for all major oxides. The whole dataset is presented as supplementary material in Supplementary Material 1 Table S1.

Density and melt viscosity were derived from the chemical composition of the analysed samples, using the models of Lange and Carmichael [1987] and Giordano et al. [2008], respectively; viscosity was obtained at T =1100 °C and 1 wt.% H_2O, corresponding to the $P-T-XH_2O$ conditions derived experimentally for the HP melt [Di Carlo 2006]; NBO/T (non-bridging oxygen per tetrahedron) was calculated using ΔNNO = +0.75, Fe^{3+}/Fe^{2+} = 0.27 and T = 1100 °C. These data are used as input parameters for Computational Fluid Dynamic (CFD) simulations and diffusion modelling.

2.2 Computational Fluid Dynamic (CFD) simulations

The mechanism and timescale of Fe-rich filaments formation were simulated using the open-source computational fluid dynamics software `OpenFOAM® (v2306)`, which has been tested and benchmarked on buoyancy-driven magma mingling [Brogi et al. 2022; Colucci et al. 2024]. The numerical simulations are performed with the multiphase solver `icoReactingMultiphaseInterFoam`, which can deal with multiple incompressible non-isothermal phases and phase change. Any exchange of mass and heat between the different phases is expected to be negligible: the system is isothermal and the two fluids (HP melt and Fe-rich melts) are assumed immiscible (see Section 4). The volume of fluid method is adopted in `OpenFOAM` to resolve the position and shape of the interface separating two fluids or phases (e.g. liquid–liquid, liquid-gas, solid-liquid). As shown by Brogi et al. [2022], the details of the numerical solver and its parameters may affect the interface geometry between liquids; however, convergence tests and comparison with other numerical solvers have demonstrated that the fluid solver reproduces well the overall dynamics of the mingling of two liquids under the effect of gravity [Brogi et al. 2022; Colucci et al. 2024].

2.3 Chemical diffusion

The temporal evolution of the concentration profile of major oxides and chlorine across filaments and host glass was modelled by generalizing Fick's second law according to Onsager formalism:

$$\frac{\partial y}{\partial t} = \mathbf{D}\left(\frac{\partial^2 y}{\partial x^2}\right), \quad (1)$$

where $\mathbf{D}$ is the diffusion matrix and y is the vector whose components are the mass fractions of the oxides in the melt. Binary diffusion coefficients (i.e. diagonal elements in $\mathbf{D}$) are well-known and estimated through laboratory experiments [Zhang and Gan 2022]. Interdiffusion coefficients (off-diagonal elements in $\mathbf{D}$) are often not determined in experiments [Guo and Zhang 2020]. In particular, at pressures (50–75 MPa) and temperatures (1100–1200 °C) of interest, interdiffusion coefficients are not available in the literature, therefore we neglect them. As a result, Equation 1 reduces to an effective binary diffusion model (i.e. $\mathbf{D}$ is a diagonal matrix) and is numerically solved in `Matlab®` with the method of lines.

Values for the binary diffusion coefficients in basaltic melts of Al_2O_3, K_2O, TiO_2, CaO, and FeO_{Tot}, in the range 1150–1500 °C, are provided by Neave et al. [2021]. For MgO and Cl, we extrapolate the diffusion coefficients from the higher temperature experiments of Guo and Zhang [2020] and Alletti et al. [2007].

3 Results

3.1 Groundmass texture

The lapilli-sized products from 11 April 2022 "normal activity" ranges from dense, equidimensional, black scoriae containing both large vesicles separated by thick septa and small vesicles that form on the external surfaces, to elongated fragments with spiny surfaces and large vesicles separated by thin septa, often with Pele's hairs endings (Figure 1A and 1B). The groundmass is porphyritic with phenocrysts of plagioclase, clinopyroxene and olivine. Plagioclase crystals are euhedral with sieved cores and oscillating zoned rims (Figure 1C). Residual glasses are homogenous and contain rare 10–100 µm-sized microlites of plagioclase (Figure 1D). The ash related to the normal activity of 29 June 2022 is mostly made up by broken crystals and lithics (Figure 1E and 1F). The juvenile fraction is represented by blocky and dark material and subordinate fluidal and light-brown fragments (Figure 1F). Groundmass is glassy with rare 10–50 µm-sized microlites of euhedral and unzoned plagioclase.

Lapilli from the 13 May 2022 "major explosion" are brown in colour with honey shades; they have an overall twisted shape, characterized by shiny and spiny surfaces that reflect the presence of highly stretched glass that ends in Pele's hairs (Figure 1G and 1H). Groundmass crystallinity is similar to the previous described samples, but the glass is not homogeneous. In this sample we detected the widespread presence of filamentary textures, characterized by a high contrast under SEM-BSE inspection, dispersed within the matrix glasses (Figure 2). Filaments have a fluidal and stretched morphology, sometimes highly convoluted, with a typically non-uniform thickness between 1 and 20 µm. They are commonly associated with vesicles (Figures 2A, 2C, 2E, 2F), where they appear to have delta-shaped endings (Figure 2A), as well as with the exter-

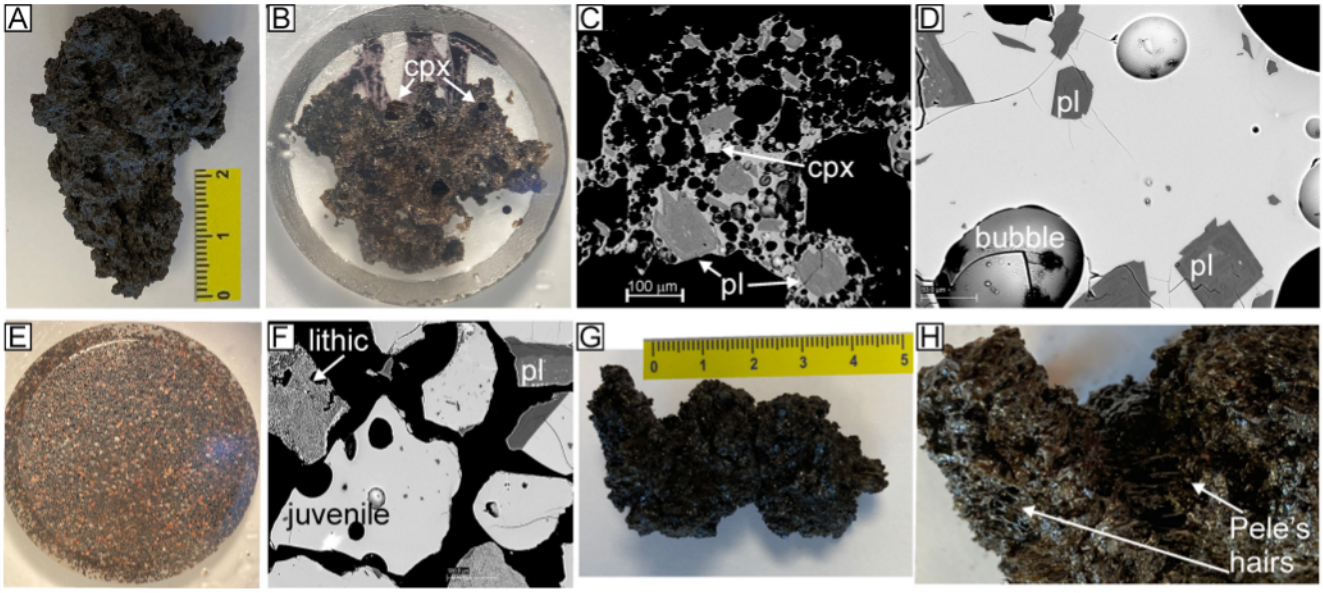

Figure 1: [A]–[D] 11 April 2022 normal activity: [A] dense lapillus; [B] 1-inch sized mount of a portion of clasts shown in [A]; (C) SEM-BSE image of groundmass texture; [D] SEM-BSE image of groundmass glass and microlites; [E]–[F] 29 June 2022 normal activity: [E] 1-inch sized mount with 0.5–1 mm ash; [F] SEM-BSE image showing juveniles, lithics and plagioclase crystals. [G]–[H] 13 May 2022 major explosion: [G] twisted-shaped lapillus; [H] particular of the clast shown in [G] with Pele's hairs on the external surface. pl = plagioclase; cpx= clinopyroxene.

nal outlines of the clasts (Figure 2H and 2I). They also show a subtle connection with the compositional boundary layers (CBLs) around plagioclase microlites (Figure 2F and 2G), and often are close to plagioclase phenocrysts (Figure 2D and 2E). Filaments can contain tiny microlites, or microlite chains, of Fe-Ti-oxides (Figure 2G). BSE-SEM images highlight that areas adjacent to the filaments commonly have a darker shade of grey than the groundmass (Figure 2A–2C and 2E), often forming dark grey filaments (Si-rich) parallel to the high-contrast Fe-rich ones (Figure 2B).

These textures were recognized in most of the analysed products from Stromboli; they are abundant and ubiquitous in the products emitted during "major explosions," including the 08 and 24 November 2009 (Figure 3A–3C), the 19 July 2020 (Figure 3D) and the 06 October 2021 events (Figure 3E). The filamentary textures described above were also observed in pumices from "paroxysms," even if this is not a distinctive character (Figure 3F). On the contrary, they are rare in lapilli from "normal activity" and never observed in the studied HP ash fraction. The same textures were observed in all the studied samples from Etna (Figure 3G–3I).

3.2 Glass geochemistry: compositional maps and transects

High-resolution X-ray maps of matrix glasses indicate that both juvenile lapilli and ash from "normal activity" at Stromboli have a homogeneous distribution of major elements, falling within the compositional field of the shallow (HP) magma, with a variation in major oxides within 2–4 % (Supplementary Material 3 Figure S1). In groundmasses from "paroxysms," mingling between LP and HP melts produces sharp contacts between zones with different elemental concentration (Supplementary Material 3 Figure S2).

The products of 13 May 2022 "major explosion" have a groundmass glass composition falling within the field depicted by the HP melts [Landi et al. 2022]. The high-contrast filaments dispersed within the groundmass are enriched in FeO_{Tot}, CaO and MgO and depleted in K_2O, SiO_2, Al_2O_3, and Cl compared to the surrounding glasses (Figure 4; Supplementary Material 3 Figure S3; Supplementary Material 1 Table S1). TiO_2 does not vary significantly from the glass (1.62 wt.% ±0.14 in HP [Landi et al. 2022]) to the filaments (1.22–1.91 wt.%). The dark-grey glasses adjacent to the filaments are Si-rich and FeO_{Tot}-poor glasses, and show an increase in K_2O (Figure 4B and 4H). Smooth elemental chemical profiles are observed in transects across the Fe-rich filaments, providing evidence of diffusion with the host melt (Figures 4D–4F and 4J–4L). As a consequence, all the analysed Fe-rich filaments share the same compositional pattern, but the absolute concentration of major elements in the filaments and in the immediately adjacent zones may vary (Figure 5). Uphill diffusion for K_2O (Figure 4B and 4H), and to a lesser extent for SiO_2, CaO, and MgO, characterizes the shape of the transects at the filament-melt interface.

Bivariate diagrams of major element oxides highlight that Fe-rich filaments measured in the products from Stromboli lie on compositional trends which diverge from the mixing line between HP and LP melts (Figure 5). Starting from different glass compositions, two trends are observed: 1) in pumices from "major explosions" associated with the emission of LP magma (e.g. 08 and 24 November 2009; 19 July 2020, 06 October 2021), Fe-rich filaments fall along the mixing line between evolved LP glass (K_2O <2.7 wt.%) and the Fe-rich CBL (FeO_{Tot} = 15 wt.%) developed at the interface between a skeletal plagioclase and the host LP glass (Figure 3F); 2) in scoriaceous

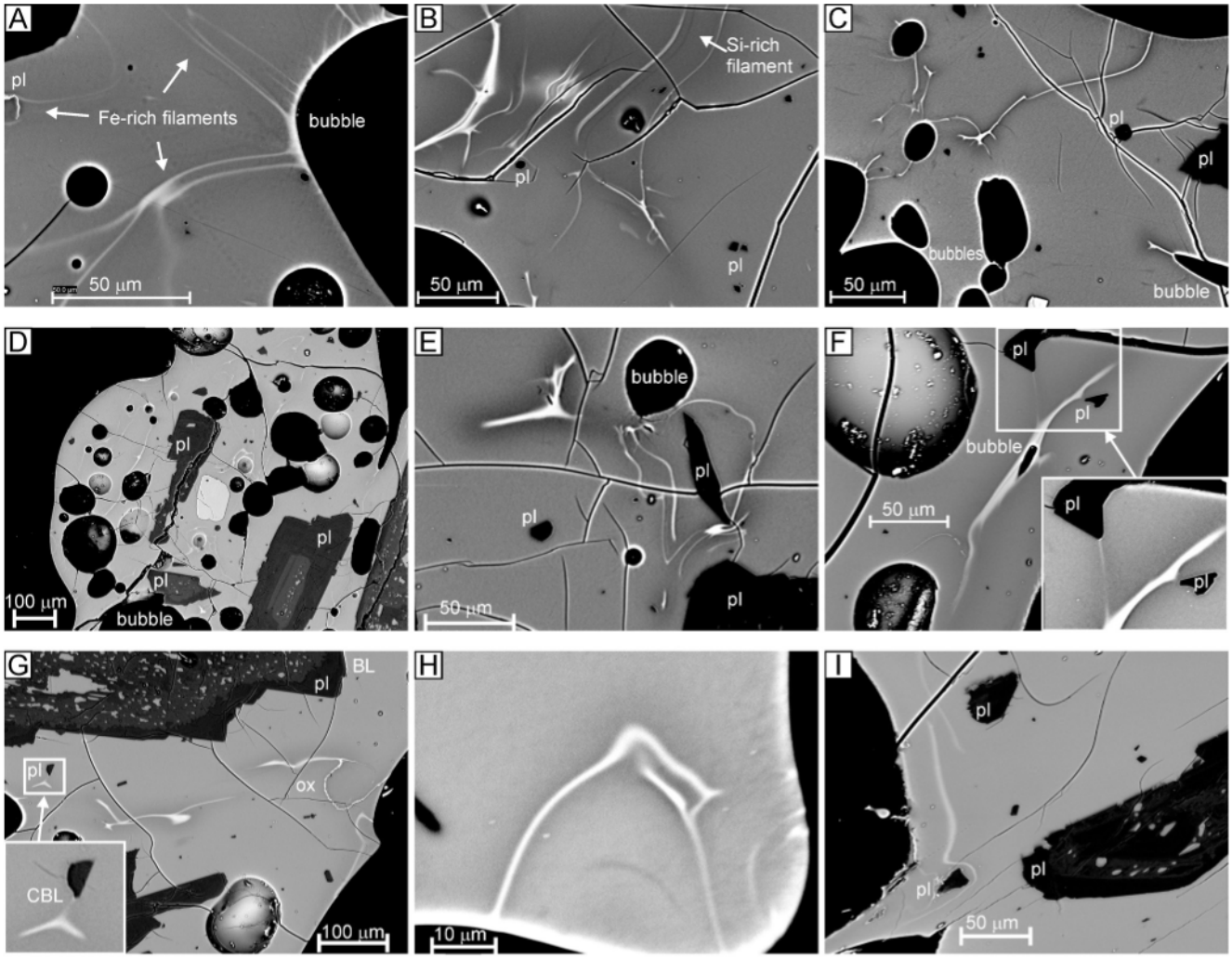

Figure 2: BSE-SEM images of the 13 May 2022 major explosion groundmass with textural details of the high-contrast, stretched and deformed Fe-rich filaments within the matrix glass. pl = plagioclase; CBL = compositional boundary layer; ox = oxides.

lapilli from "major explosions," in which the LP end-member has not been detected (e.g. 13 May 2022), an almost parallel line to the previous one connects the averaged HP glass composition and the Fe-rich filament with FeO_{Tot} = 19 wt.%. In some samples, the filaments fall on both trends, and these are samples from "major explosions" characterized by mingling between HP and LP, and by intermediate glass compositions (08/11/2009;19/07/2020). The zones between the Fe-rich filaments and the host glasses are characterized by Si-rich and K_2O-rich compositions, that reach values up to 56.8 wt.% and 5.7 wt.%, respectively (Figure 5A and 5B). Chlorine is strongly depleted in Fe-rich filaments (<0.08 wt.%) (Supplementary Material 3 Figure S3), while TiO_2 does not show variations, falling within the field of variation of the HP melts (Figure 4E and 4K; Supplementary Material 1 Table S1).

At Etna, the Fe-rich filaments show similar compositional trends described above, starting from different glass compositions (Supplementary Material 3 Figure S4).

3.3 Computational Fluid Dynamic (CFD) simulations

Figure 6 shows the space-time evolution of our 2D numerical setup: a rectangular plagioclase crystal surrounded by a shell of heavy liquid, the CBL, immersed in the less dense host HP melt. Sizes and physical properties calculated from chemical composition analyses are reported in Table 1. The initial geometry and sizes of the crystal and the CBL have been chosen to be consistent with observations. The density and viscosity of the two liquids are kept constant during the simulation and the density of the crystal and of the HP melt is assumed to be the same. The solid phase is modelled as a very viscous

Table 1: Physical parameters for the multiphase flow simulations.

Parameter	Value	Unit
crystal length	100	µm
crystal width	26	µm
CBL width - long crystal side	10	µm
CBL width - short crystal side	5	µm
crystal and HP melt density	2510	$kg\,m^{-3}$
CBL density	2790	$kg\,m^{-3}$
HP melt viscosity	2.5	(log, Pa s)
CBL viscosity	2.05	(log, Pa s)

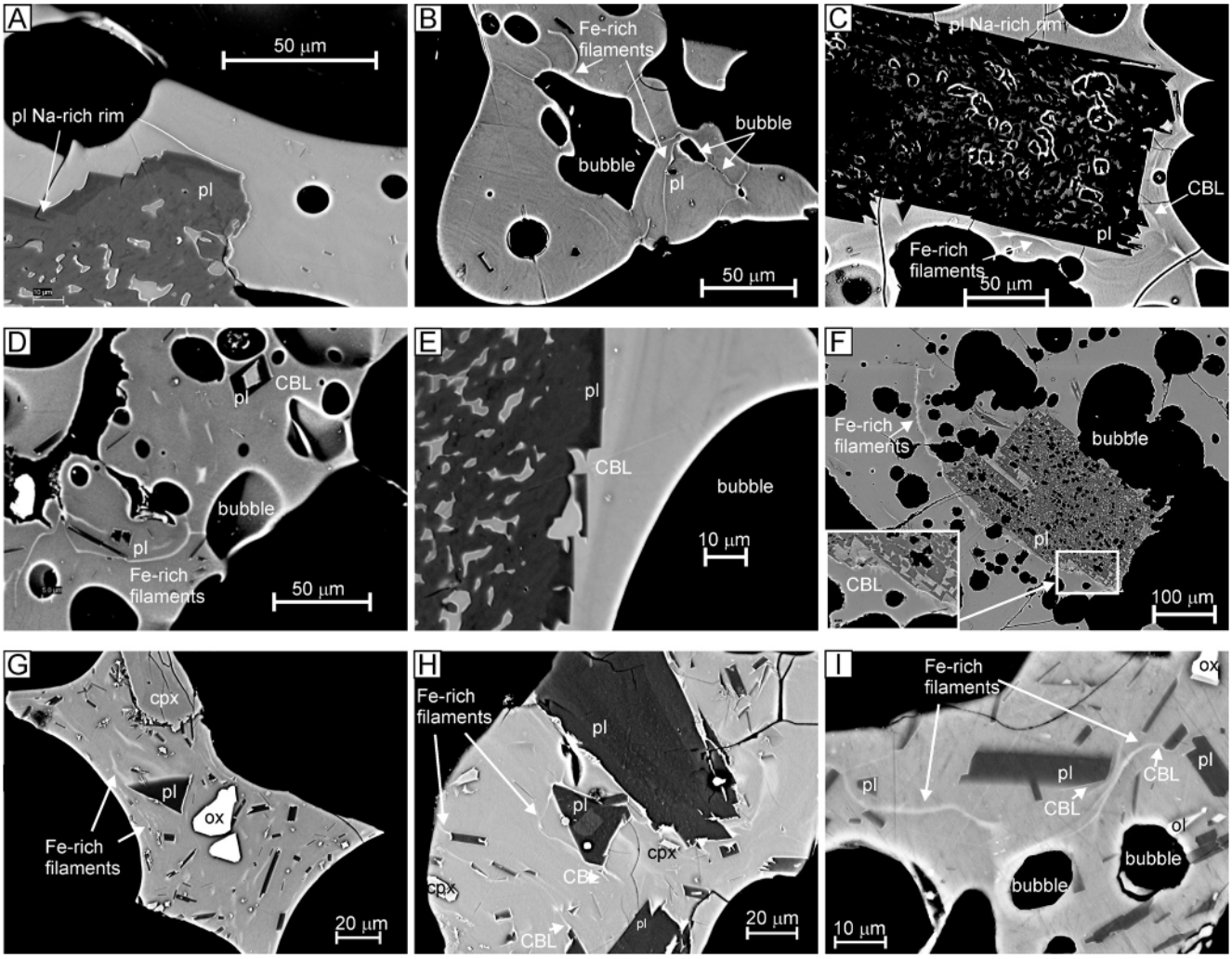

Figure 3: SEM-BSE images of Fe-rich filamentary textures in groundmass glasses from Stromboli [A]–[F] and Etna [G–I]: [A]–[B] 08/11/2009 major explosion (La Felice and Landi, 2011); [C] 24/11/2009 (ME) [La Felice and Landi 2011]; [D] 19/07/2020 major explosion [Landi et al. 2022; Voloschina et al. 2023]; [E] 06/10/2021 major explosion [Landi et al. 2022]; [F] 03/07/2019 paroxysm [Andronico et al. 2021]; [G] 24/12/2018 powerful Strombolian-like explosion [D'Oriano et al. 2022]; [H] 23/01/2019 ash rich emission [D'Oriano et al. 2022]. [I] 24/03/2022 [Andronico et al. 2024]; pl = plagioclase; cpx= clinopyroxene; ox = oxides; CBL = compositional boundary layer.

liquid, such that during the time interval of our simulations, it does not undergo any shear deformation. For simplicity, interfacial forces between the two liquids (interface tension) and solid (wetting forces) are neglected since coefficients for these forces are not well known, preventing a quantitative assessment of their effects. Non-negligible interfacial forces might slow down the detachment process, up to inhibiting formation of the stretched filaments. Any effect due to crystal roughness is not considered for simplicity. Therefore, gravity and viscous forces are driving the observed multiphase fluid dynamics. Figure 6 shows that the CBLs sink into the host HP melt due to their higher density. As they detach from the crystals, they form filamentary textures with non-homogeneous sizes. Filaments show typical Rayleigh-Taylor instability patterns (Figure 6), accumulating in droplets that are sometimes larger than the initial CBL width. CBLs start separating from the crystals on timescales of hours; complete removal is not observed in our simulations, but their width is considerably reduced after a few days, and filaments are well dispersed within the melt on this timescale.

The timescale for filaments to start sinking by gravity into the host HP melt can be evaluated, to first approximation, as the inverse of the viscous Rayleigh-Taylor instability growth rate γ [Bellman and Pennington 1954]. The latter can be expressed as:

$$\gamma = \frac{(gA)^{2/3}}{\nu^{1/3}}, \qquad (2)$$

where A is the Atwood number $A = (\rho 1 - \rho 2)/(\rho 1 + \rho 2)$ and ν is the density-weighted average viscosity $\nu = (\eta 1 + \eta 2)/(\rho 1 + \rho 2)$. Given the densities and viscosities calculated from the melt compositions (Table 1), the timescale for filament detachment is on the order of 10 s, confirming that the process is favoured in these conditions.

We performed numerical simulations considering two different angles of the crystal with respect to the vertical axis (parallel to gravity force) (Figure 6A and 6B). The initial ori-

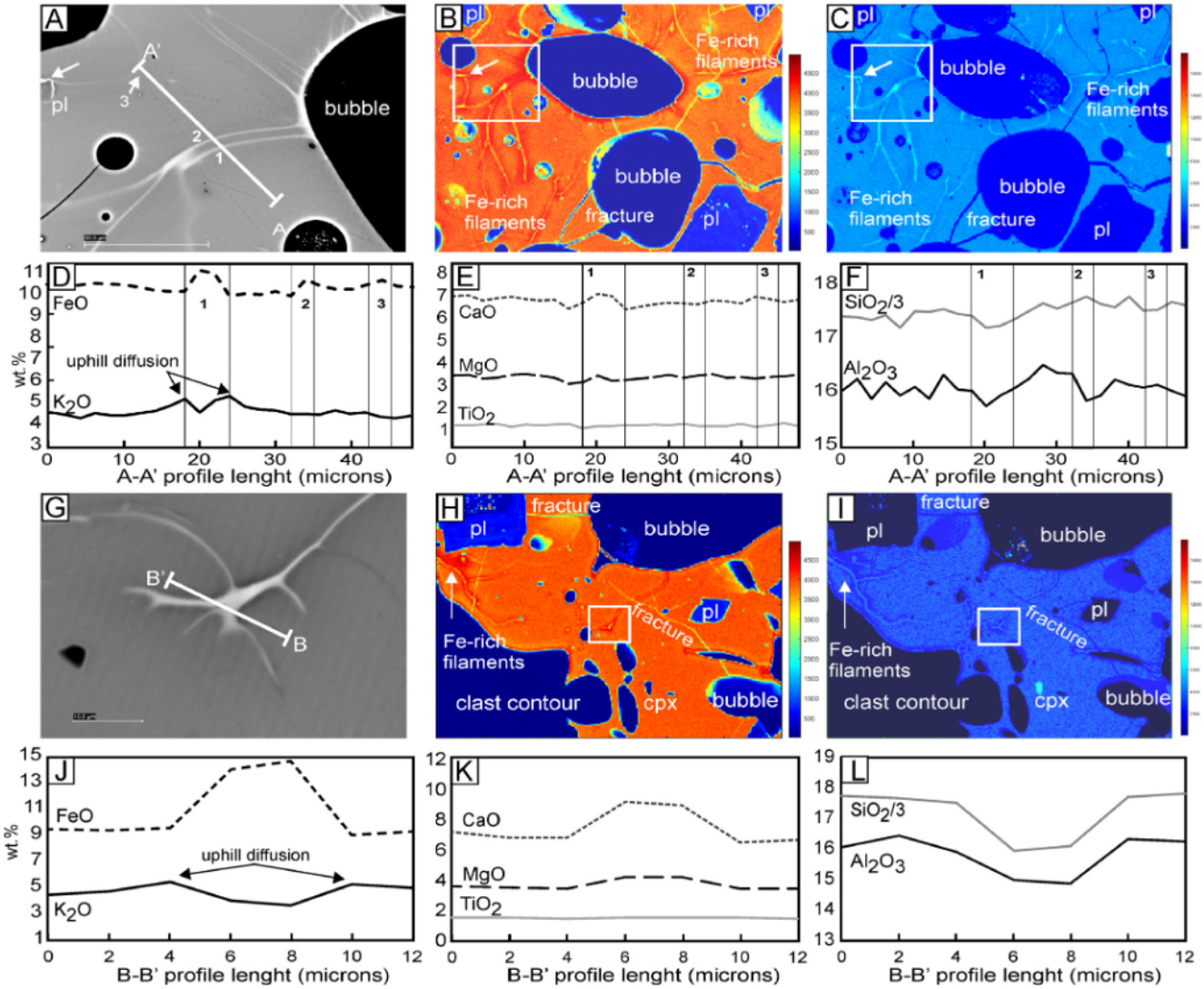

Figure 4: Compositional features of the Fe-rich filamentary textures from the 13/05/2022 major explosion. [A] and [G] BSE-SEM images; [B] and [H] K_2O compositional maps; [C] and [I] FeO_{Tot} compositional maps; [D]–[F] and [J]–[L] compositional profiles across filaments. A–A', B–B' indicate the track of compositional profiles. White areas in [B], [C], [H], [E] correspond to BSE-SEM images on the left; white arrows indicate a plagioclase connected with a Fe-rich filament. SiO_2 wt.% was divided by 3 for a scale issue. pl= plagioclase; cpx= clinopyroxene. The fractures are an artefact related to sample preparation and are filled with epoxy resin.

entation of the crystal changes the details of the topological evolution of the filaments but, overall, it does not significantly affect the average filament thickness or the timescale of the detachment and mingling processes. In nature, the simulated system cannot be considered static over a period of days; however, given its small size, we can assume that it is transported as a whole by large convective motions within the magmatic reservoir. The crystal could thus be reoriented with respect to the gravity force, while the CBL is sinking, possibly contributing to more complex flow patterns. Although our simulations do not represent this scenario, we expect that gradual reorientation of the crystal does not significantly change the outcome of our simulations, in terms of overall dynamics and timescales. This conclusion is also supported by the results from simulations for different crystal angles with respect to gravity.

3.4 Diffusion modelling

Figure 7 shows the concentration profile of the Fe-rich filament analysed in the 13 May 2022 "major explosion" (13may22_2b profile1# in Figure 4E–4L; Supplementary Material 1 Table S1) considered for testing the diffusive processes between the host melt and the filaments. The diffusion timescale τ is directly proportional to the square of the filament's thickness L and inversely proportional to the diffusion coefficient $\mathcal{D}$ ($\tau \sim L^2/\mathcal{D}$). Considering filaments thicknesses of 1–10 μm and diffusion coefficients for different species from 10^{-12} to 10^{-13} $m^2\,s^{-1}$, the diffusion timescale lies in the range of 1–100 s. To better pinpoint this timescale, we perform a numerical simulation for a single profile measured in the selected sample, containing enough measurement points to be modelled (Figure 7; Colucci [2025]). Possible analytical convolution effects that may influence narrow objects by stretching

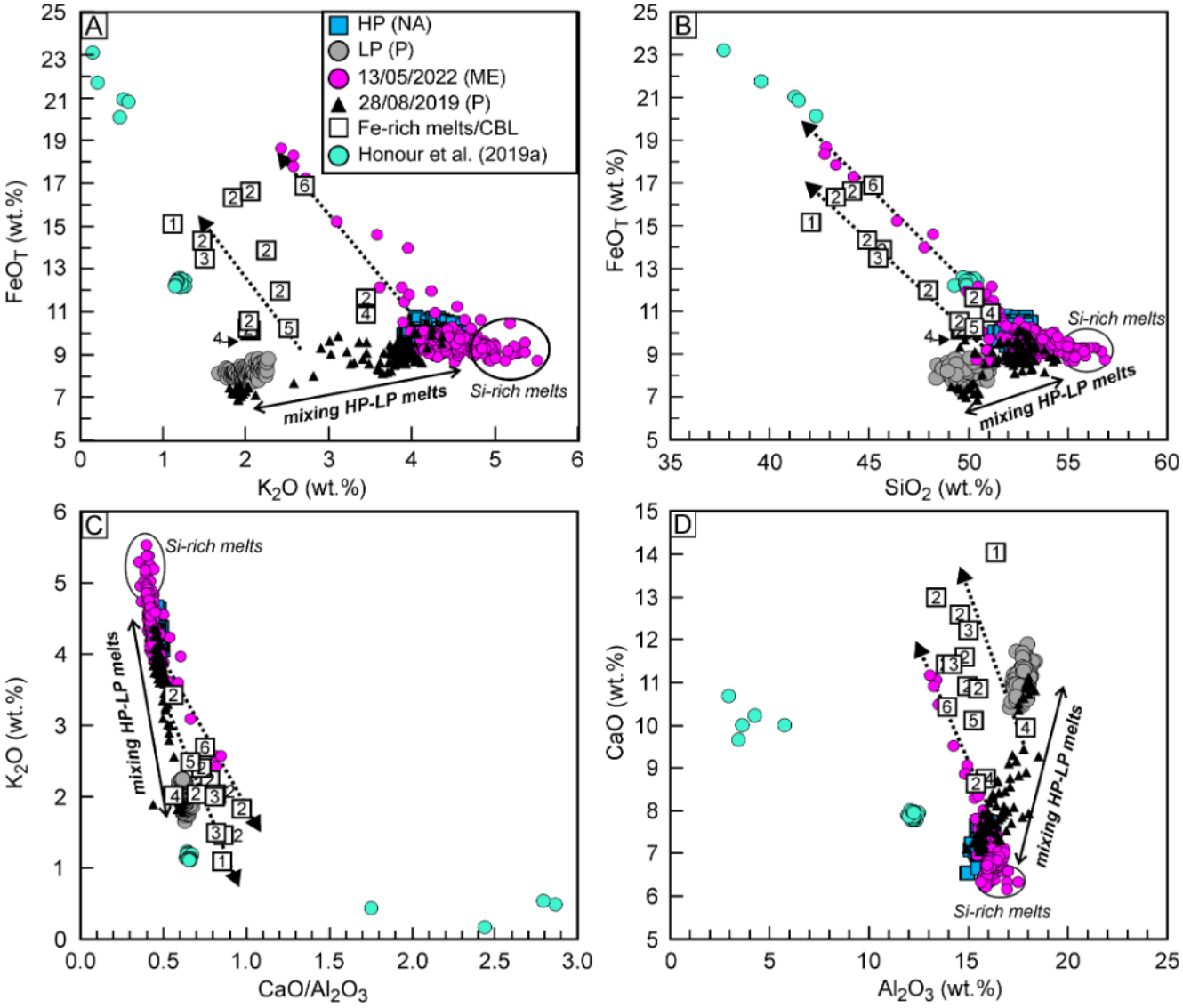

Figure 5: Bivariate compositional diagrams. HP (NA) and LP (P) data are from Landi et al. [2022]. Fe-rich melts/CBL (numbered white squares) were measured in: (1) 03/07/2019 (P); (2) 08/11/2009 (ME); (3) 24/11/2009 (ME); (4) 19/07/2020 (ME); (5) 06/10/2020 (ME); (6) 13/05/2022 (ME). 13/05/2022 (ME) and 28/08/2019 (P) datasets include analyses acquired on transects across Fe-rich filaments. The double arrow represents the mixing line between LP and HP magmas at Stromboli. In all diagrams, the compositional patterns depicted by Fe-rich melts (dotted arrows) are far from the magma mixing. We identified two trends, starting from two different glass compositions: the evolved LP and the mean HP, respectively. There is also a correspondence between the Fe-rich filaments, the compositional boundary layer (CBL) and the crystal-growing melt. Si-rich field groups the analyses performed on the dark grey melts adjacent to the Fe-rich filaments. For comparison, a selection of data from Honour et al. [2019a] is also reported. NA = normal activity; ME = major explosion; P = paroxysm.

the measured concentration profiles were evaluated with the PACE model of Jollands [2020]. The results indicate that these effects are negligible and always within the uncertainty range of the diffusion coefficients, so we can exclude them.

The diffusion between a filament and the host melt was modelled by considering the composition reported in Supplementary Material 1 Table S1, at 1150 °C. As initial conditions, we assume a double step function, i.e. the filament and host melt are delimited by a vertical contact discontinuity with flat profiles on their respective domains. As diffusion proceeds, it reduces the compositional gradient, progressively smoothing the discontinuity. The numerical simulation was stopped when the computed profile matched the measured one. Despite the uncertainties associated with diffusion coefficients and initial conditions, there is a qualitative agreement between observed and modelled concentration profiles after 5 s (Figure 7). Agreement between data and model deteriorates for oxide profiles characterised by evident interdiffusion phenomena, e.g. for K_2O, which presents uphill diffusion (Figure 7C). We then consider the time required for the filament to completely disappear, that is when the concentration profiles

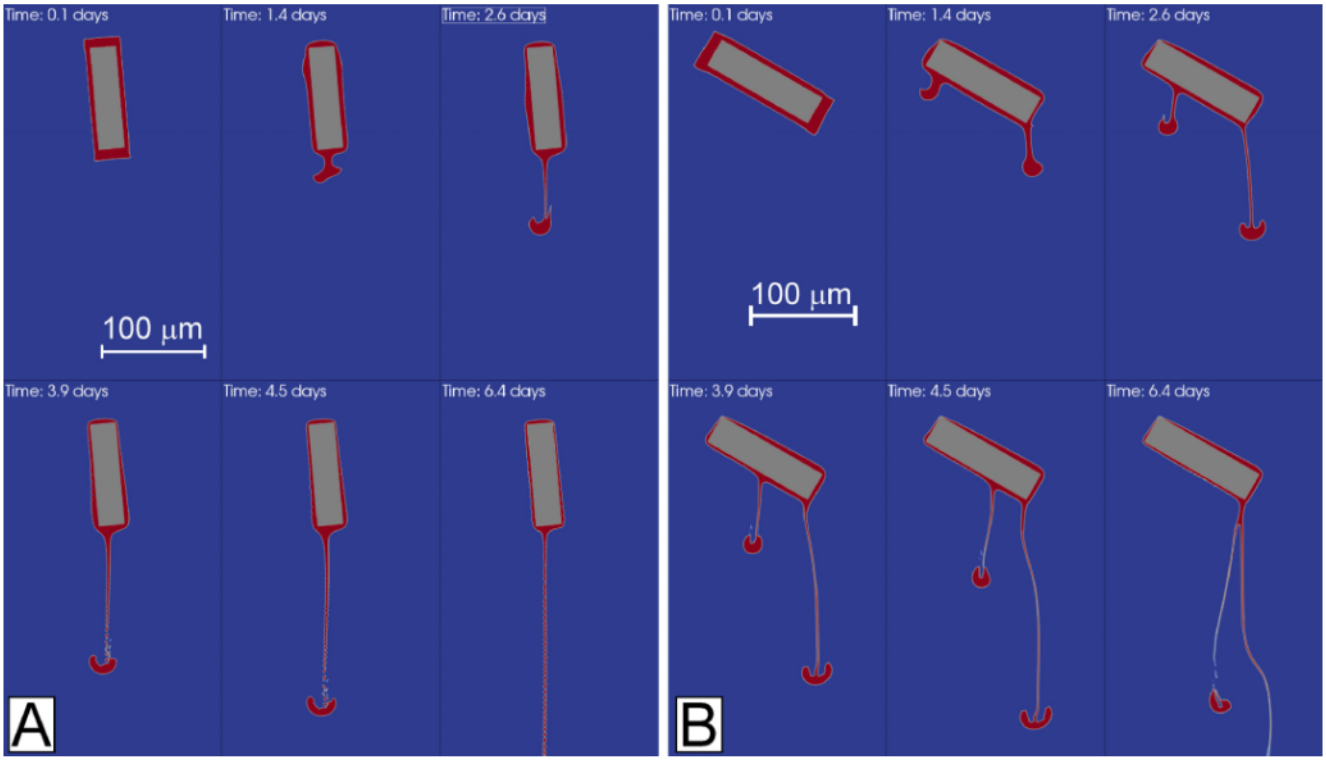

Figure 6: [A] Evolution of a CBL (red) as it detaches from a plagioclase crystal (grey) and sinks into the host HP melt (blue). [B] The long-axis of the plagioclase crystal is rotated of 60° with respect to the vertical axis.

become flat: this condition is reached after ~400 s, consistent with the estimate based on the scale analysis.

4 Discussion

4.1 The origin of the Fe-rich compositions in basaltic magmas

To understand the origin of the Fe-rich filaments within basaltic glasses, we examined all the compositions present within the studied systems, which are possibly compatible with those of the filaments. We exclude that these correspond to primitive mafic melts, as suggested by González-García et al. [2023] for the 2021 Tajogaite eruption of Cumbre Vieja (Canary Islands, Spain), since, at Stromboli, the most mafic end-member (LP) involved in all the "paroxysms" and in some of the "major explosions" has a FeO_{Tot} content lower than 10 wt.%, in contrast with the higher (up to 19 wt.%) FeO_{Tot} of the filaments (Figure 5A and 5B). We cannot exclude that analyses were contaminated by Fe-Ti oxide nanolites [Di Genova et al. 2020; González-García et al. 2023; Di Fiore et al. 2024] that have crystallized inside the filaments after their formation. However, we would like to stress that the chemical composition of the Fe-rich filaments is different from that of LP melt also for its Al_2O_3 content (Figure 5D), which is higher in the LP glasses from Stromboli (17.7 ± 0.3 wt.% [Landi et al. 2022]) compared to that measured in the filaments (13.3–16.4 wt.%).

To take into account the contribution of partial melting/dissolution processes occurring at the interaction between the intruding LP magma and the upper crystal mush, we examined Fe-rich mineral phases that could contribute to the Fe-rich composition of the filaments, such as Fe-Ti oxides, clinopyroxene and olivine. Fe-Ti oxide minerals are not present in Stromboli magmas, except in lithic particles, while, at Etna, Fe-Ti oxides can crystallize at magmatic conditions. However, their dissolution (either lithics or Fe-Ti oxides) would not explain the low content of TiO_2 in filaments (2.0–3.7 wt.% in Etna products) and its slight increase in the filaments (up to 1.2 and 2.6 wt.%) with respect to the residual glasses at Stromboli (0.96 wt.% on average in LP; 1.62 wt.% on average in HP).

At Stromboli, the highest Fe-rich pyroxene composition was measured in resorbed cores of crystals with Mg#70 and Fs_{18} [Landi et al. 2022]. Computed mass balance assimilation (Supplementary Material 2 Table S2) indicates that the FeO_{Tot} contents measured in filaments cannot be achieved even by completely melting these cores, so the hypothesis that Fe-rich filaments represent partial melting of this mineral phase can be rejected. Similarly, olivines have high FeO_{Tot} content (up to 27 wt.% in Fo_{70} [Landi et al. 2022]), and, in some products from "paroxysm" at Stromboli, Fe-rich melt inclusions have been reported in $Fo_{80–90}$ olivines in equilibrium with LP melts. Bertagnini et al. [2003] proposed that FeO_{Tot}-rich melt inclusions result from the dissolution of pre-existing olivines ($Fo_{70–75}$) following the interaction between the LP and HP magmas. In our samples, the increase of CaO content from LP and HP melts towards the centre of the filaments (Figure 4) is incompatible with olivine assimilation. Nevertheless, during "major explosions" and "paroxysms" at Stromboli, resorbed Fs_{18} and Fo_{71} cores surrounded by less evolved compositions in equilibrium with the LP magma are often emitted. Thus,

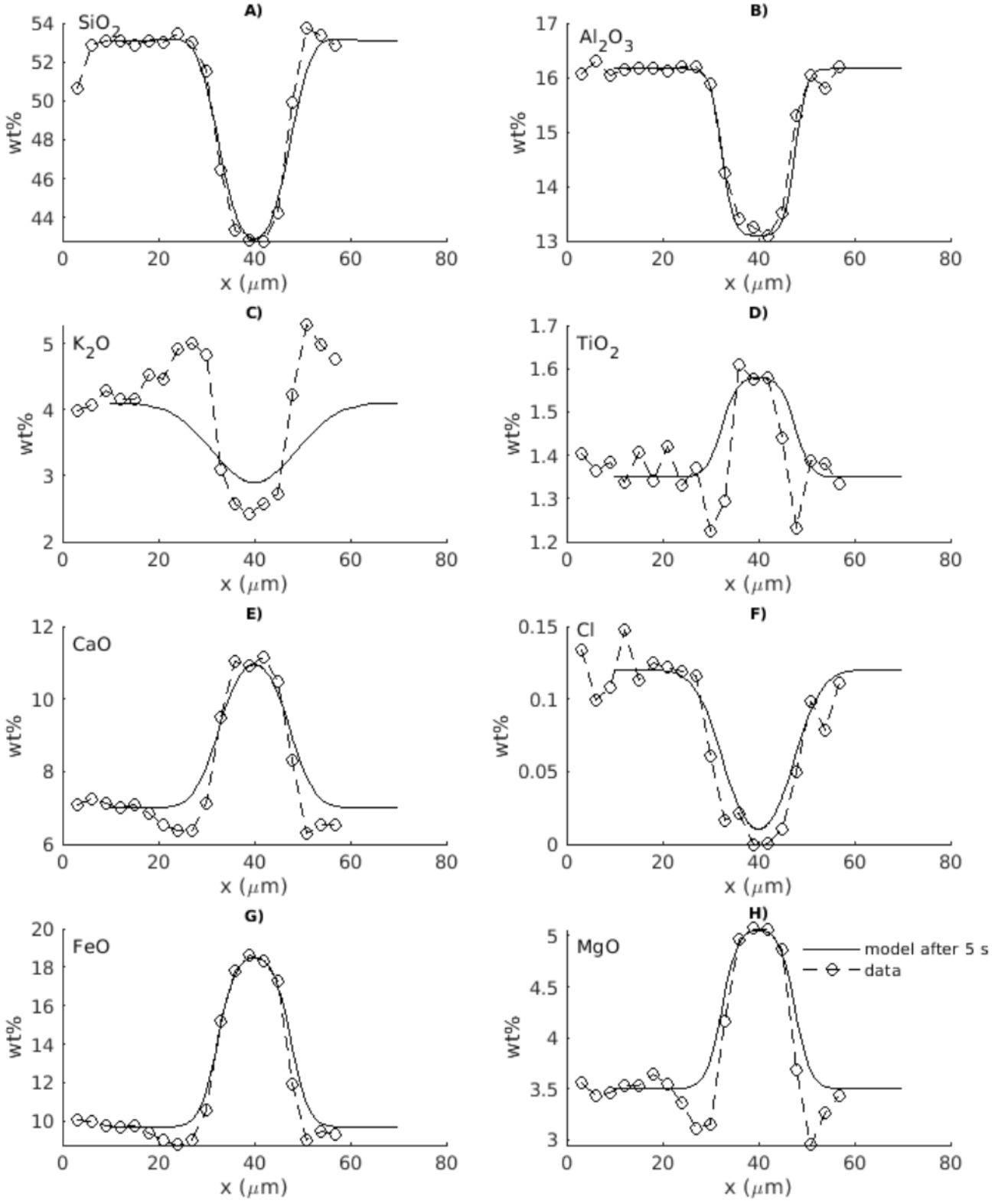

Figure 7: Modelling results of elemental diffusion. Circles are the measured concentrations along profiles (sample 13may22_2b profile1# in Supplementary Material 1 Table S1; Figure 4G–4L) connected by dashed lines. Solid lines are the modelled concentration profiles after 5 s. Best fit diffusion coefficients: Al_2O_3 = 4.2 × 10^{-13} m s^{-2}; K_2O = 51 × 10^{-13} m s^{-2}; TiO_2 = 6.9 × 10^{-13} m s^{-2}; CaO = 15.4 × 10^{-13} m s^{-2}; Cl = 20 × 10^{-13} m s^{-2}; FeO= 8.9 × 10^{-13} m s^{-2}; MgO = 7.2 × 10^{-13} m s^{-2}.

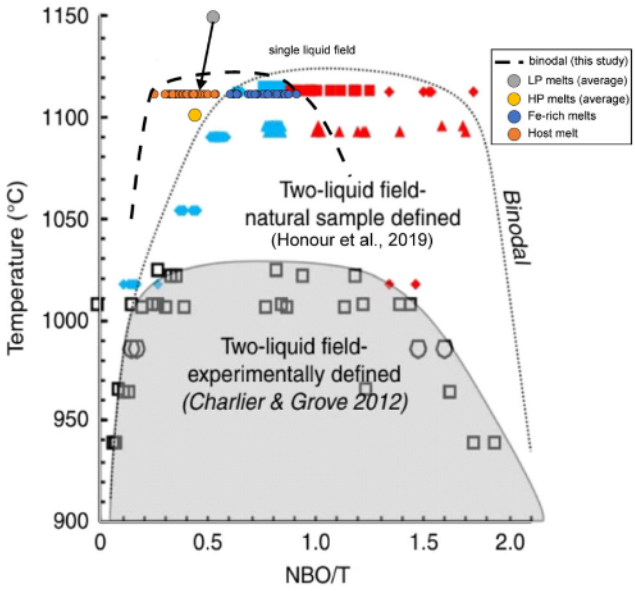

Figure 8: Diagram modified after Honour et al. [2019a] showing the NBO/T against Temperature (*T*) for melts analyzed in products from the 13 May 2022 "major explosions" at Stromboli (the present work) compared with those obtained on natural [Honour et al. 2019a] and experimental samples [Charlier and Grove 2012]. Starting from the averaged values of LP melts [Landi et al. 2022], the arrow indicates the liquid line of descent from 1150 °C to 1100 °C, the latter corresponding to the averaged composition of HP melts [Landi et al. 2022]. Fe-rich melts and host melts are plotted considering a *T* of 1110 °C for a convenience of visualization. Actually, we cannot precisely know the T of these melts, but we suppose that they are close to HP, and between LP and HP magmas. The shift of the binodal curve toward low NBO/T values with respect to that depicted by Honour et al. [2019a] is due to the high pressure (75–50 MPa), and consequently low Fe^{2+}/Fe^{3+} ratio, used for obtaining NBO/T.

we cannot exclude that the intrusion of LP magma may induce the partial melting of both evolved clinopyroxene and olivine present in the shallow reservoir (< 3 km depth) forming liquids that may contribute to the composition of the Fe-rich filaments (Supplementary Material 2 Table S2; Supplementary Material 3 Figure S4).

Petrological results obtained in the present work indicate that studied products contain microlites and phenocrysts of plagioclase with a wide range of textures and compositions. Plagioclase microlites can be either euhedral and swallowtail in shape and in both cases they can develop high-contrast CBLs at the melt-mineral interface. Similarly, CBLs with chemical compositions in trend with the measured Fe-rich filaments also characterize plagioclase phenocrysts that undergo dissolution/recrystallization, following LP-HP interaction [Pichavant et al. 2022] (Figures 2, 3A, 3E, 3F and 5; Supplementary Material 1 Table S1). The formation of CBLs at the plagioclase-melt interface is a well-known process, promoted by an increase in the growth/dissolution rates of crystals, which exceed the diffusion rate of ions from the melt to the crystals [Zellmer et al. 2016]. In the andesitic tephra from the Taupo Volcanic Zone, Ca-rich bands were observed in some pyroxene microantecrysts [Lormand et al. 2021]. These Ca-rich rims are different from that measured in our products, as they are also enriched in Cr, Fe, Ti, but not in Mg. Lormand et al. [2021] related them both to rapid cooling at depth, due to a high temperature gradient between the intruding melt and the dyke walls, and to shallow ascent of H_2O-saturated melts, resulting in heating through latent heat release of microlite crystallisation. In basaltic magmas, the absence of dendritic textures associated with fast cooling or undercooling rates has been related to relatively high water concentrations in the melts [Shea and Hammer 2013]. This could explain why the formation of CBLs also occurs on euhedral microlites rapidly growing at depth.

Honour et al. [2019a,b] identified CBLs at plagioclase-melt interface as the origin of Fe-rich immiscible droplets in the Kilauea Iki lava lake, and related them to the crystallization by cooling of a plagioclase mush. The same process has been considered responsible also for the generation of Si-rich and K_2O-rich melts, as reported by Charlier and Grove [2012] during crystallization experiments of tholeiitic basalts.

The similarity between the composition of the Fe-rich CBLs developed at the melt-plagioclase interface and that of the Fe-rich filaments led us to explore the possibility that they are genetically related.

4.2 Mechanisms and timescales for the formation of Fe-rich filaments

Textural, geochemical, and modelling results obtained in the present study suggest that Fe-rich filaments represent the evolution of CBLs generated at the plagioclase-melt interface. The subtle connection of filaments with microlites also supports this interpretation (Figure 2F–2G; Figure 3). An interesting correspondence also emerges by comparing our Fe-rich filaments with the results of the mixing experiments conducted by Laumonier et al. [2014] at high-pressure between anhydrous mafic and felsic magmas. The authors found "anomalous" Si-poor and FeO-, MgO-, and CaO-rich melt compositions in experiments performed under static conditions, and for experimental duration (50 h) comparable to the timescales derived from our simulations. These melt pockets characterize the interaction zones close to the mafic end-member, and are adjacent to plagioclase phenocrysts that have crystallized Na-rich external rims. The authors interpreted them as the result of a higher local melt fraction in the reaction zones between the two end-members, reflecting local heterogeneities of the initial modal composition of the basalt (e.g. higher fraction of olivine and/or pyroxene). However, the complete absence of filaments in the 3-h static experiments, where plagioclase crystals are unzoned, together with their constant presence in plagioclase-rich zones, again suggests that Fe-rich melts and CBL are correlated.

CFD simulations show that, given the higher density of Fe-rich CBL compared to the surrounding melt, the action of gravity alone explains its separation from the crystal. Moreover, simulations show that the CBL sinks into the host melt forming fluidal filaments that disperse in patterns akin to those observed in the analysed samples (Figure 3). The timescale for

the dispersion of filaments from CBLs is in the order of a few days. These estimates may be taken as indicative, as further investigations with a 3D model are required to better constrain these values. Nevertheless, volume forces (gravity) and viscous forces that drive the dynamics scale in the same way from 2D to 3D; Garg and Papale [2022] demonstrated that 2D and 3D simulations provide similar results for gravity-driven viscous flows.

Derived timescales are well in agreement with Fe-Mg diffusion timescales obtained for olivine crystals [Voloschina et al. 2023] and clinopyroxene [Petrone et al. 2022] erupted at Stromboli during "major explosions" (19 July 2020 and 25 June 2019) and "paroxysms" (3 and 28 August 2019). These previous studies indicated pre-eruptive magmas interaction (i.e. recharge of LP from depth and mixing with the resident HP) between few days and months/years.

On the other hand, experiments aimed at reproducing plagioclase reaction textures during the interaction between the HP and LP magmas suggest incubation times preceding "major explosions" and "paroxysms" at Stromboli by a few hours [Pichavant et al. 2022]. The differences in the timescales obtained with the CFD (few days) and the experiments (hours) could be explained by taking into account that: 1) the experimental data underestimate the timescales because after magmas interaction and degassing, which rapidly leads to the dissolution of pre-existing An-rich plagioclase and growth of new Na-rich rims (hours), the natural system, at least before the major explosions, can approach the equilibrium by slowing dissolution/growth rates allowing the CBL detachment from the crystals; 2) our model consider the plagioclase-CBL-host melt as a static system which result in an excess of the estimated time.

Timescales derived from diffusion modelling of elemental concentration profiles span from seconds to minutes (Figure 7). If diffusion was a dominant process, CBL filaments would disappear as soon as they separate from the plagioclase. Filaments can instead be observed in many products from explosive eruptions at basaltic volcanoes, indicating a possible role for melt immiscibility. A possible explanation is the drastic reduction of the diffusion coefficient due to the metastable immiscibility of the Fe-rich filaments with the host melt. In the NBO/T against temperature diagram (Figure 8), our samples intersect the immiscibility region, delimited by the binodal curve, identified by Honour et al. [2019a,b] for basaltic compositions. When the binodal curve lies beneath the liquidus, as in our case, then the immiscibility gap is metastable [e.g. Veksler and Charlier 2015] implying that elemental diffusion is slowed down, even if not completely absent. The uphill diffusion observed in both transects and EMPA compositional maps obtained in our study can be considered as further evidence of liquid immiscibility [Cahn 1961; Honour 2020]. If we consider this hypothesis plausible, in different volcanic contexts, such as Etna and Stromboli, we should expect filaments with different oxide concentrations, but with similar trends, as observed in the present study, since the hosting melts have different compositions [Charlier and Grove 2012].

We hypothesize that, because of the metastable immiscibility, chemical diffusion slows down by at least five orders of magnitude, allowing the filaments to survive after separation from crystals. Specifically designed experiments on the formation and evolution of boundary layers are currently missing but could significantly enhance our understanding of the mechanisms behind Fe-rich filament development. We encourage future experimental studies to define potential $P-T-X$ intervals and dynamics associated with the formation of Fe-rich filaments. Moreover, since anhydrous, low-pressure conditions typically favour immiscibility [Charlier and Grove 2012; Honour et al. 2019a], further experiments will also provide the exact position of the immiscibility gap in the phase diagram at increasing pressure and water contents. It is worth on nothing that, although high pressure expands the stability field of augite, and hence early iron enrichment of the liquid is inhibited [Grove and Baker 1984; Grove et al. 1992; Villiger et al. 2004; 2006], this effect is compound as plagioclase crystallisation affects the concentration of elements which expand the silicate liquid immiscibility field [Honour 2020].

4.3 Volcanological implications

Conditions for disequilibrium crystallization of plagioclase in basalts can be achieved during high decompression rate and high undercooling [La Spina et al. 2016; Mollo and Hammer 2017]. At Stromboli, the intrusion of LP magma at the base of the HP reservoir (75–50 MPa) is accompanied by ascent-related degassing, which results in a degree of undercooling (ΔT ~25 °C) that promotes rapid (<1 h) crystallization of plagioclase microlites [Arzilli et al. 2015; Le Gall and Pichavant 2016]. At the same time, the dissolution of pre-existing An-poor phenocrysts and the rapid crystallization of the An-rich component accompany the interaction between the two magmas, and has been already recognized at Stromboli as responsible for CBLs development around plagioclase phenocrysts [Landi et al. 2004; Pichavant et al. 2022]. Similar thermal conditions (T, ΔT) derived by Honour et al. [2019a,b] for the immiscible Fe-rich droplets formations are compatible with the LP magma (T =1150 °C) entering at the base of the shallow HP system (T =1120–1100 °C).

The proposed mechanism for the formation of Fe-rich filaments supports the idea that the interaction between LP and HP magmas occur a few days at intermediate depths (<75 MPa, ~3 km) before "major explosions" at Stromboli [Landi et al. 2022; Petrone et al. 2022; Voloschina et al. 2023]. Existing experimental studies indicate that, if the LP magma evolves by crystallization and degassing around 50 MPa, after an initial volatile loss, the H_2O-crystal-melt system can reach equilibrium in a few hours. Therefore, if interaction conditions persist for a few days, CBLs have sufficient time to detach from plagioclase and disperse as a metastable immiscible melts into the resident magma. The inferred timescales of days should be considered an upper limit, since bubbles can promote the folding and stretching of filaments [Wiesmaier et al. 2015], accelerating their diffusive mixing with resident spindles, especially during the final and fastest ascent to the surface.

One of the most relevant implications of this study concerns the non-uniform magma ascent rate along the Stromboli plumbing system, at least before the "major explosions".

We would like to underline that the magma rising from depth should spend a few days in the interaction zone, where crystallization, gas accumulation, and the consequent collapse of the foam occur [Landi et al. 2022; Petrone et al. 2022; Voloschina et al. 2023]. The triggering of the "major explosions" at Stromboli seems to occur at this depth range (<75 MPa [Landi et al. 2022; Voloschina et al. 2023]), and this should be considered in the conceptual models that underlie the interpretation of the geophysical and geochemical signals [Aiuppa et al. 2021; Ripepe et al. 2021; Pichavant et al. 2022; Voloschina et al. 2023].

After their formation, the presence of Fe-rich filaments can contribute to increasing explosivity twofold: by promoting bubble nucleation and by modifying the rheology of the magma. As suggested by González-García et al. [2023], Fe-rich filaments can be dragged by gas bubbles toward the upper portions of the conduit, where they are subjected to conditions of increased oxygen fugacity. This could facilitate the crystallization of Fe-Ti-oxides within the Fe-rich filaments, which may represent zones of local weakness in the magma where fractures can easily propagate within the upper conduit [Taddeucci et al. 2021] or at the fragmentation level [Hornby et al. 2024]. In turn, it has been shown that the presence of micron-sized Fe-Ti oxides favours the heterogeneous nucleation of bubbles [Cáceres et al. 2020; Di Genova et al. 2020] which could be crucial for the fragmentation of magma [Knafelc et al. 2022; Valdivia et al. 2023; Yoshida et al. 2023].

5 Summary and Conclusions

In this study, we propose a potential mechanism to explain the formation of micro-textures commonly observed in products from high-energy explosive eruptions at basaltic volcanoes. These micro-textures are characterized by Fe-rich filaments dispersed within the host glass, which have been analyzed in terms of their textural and compositional properties. The mechanisms underlying their formation and the timescales for their preservation are investigated using computational fluid dynamics and diffusion modeling.

In summary:

- Fe-rich filamentary textures are abundant in the products of the "major explosions" at Stromboli, and at Etna in the products associated with a powerful Strombolian-type eruption (24 December 2018) and in the ash emitted at the beginning of long-lasting, continuous emissions at the NEC (23 January 2019).

- High-resolution X-ray chemical maps, compositional transects and spot analyses reveal that Fe-rich filaments correspond to compositional boundary layers (CBLs) developed at the plagioclase-melt interface when the interaction between magmas with different temperature and volatile contents cause disequilibrium crystal growth.

- Fluid dynamic calculations have highlighted that CBLs can detach from plagioclase crystals and sink and disperse inside the host melts under the action of gravity alone.

- Fe-rich filaments are metastable immiscible melts that can therefore survive for a while after their formation without diffusing into the host melt.

- The timescales for Fe-rich filaments formation and dispersion within the host melt are of the order of a few days. The derived timescales are of the same order as those obtained through petrological data for pre-eruptive interaction between HP and LP magmas at Stromboli.

- Fe-rich filaments can contribute to increasing explosivity by promoting bubble nucleation and by modifying the rheology of the magma.

- Analogy with other basaltic systems leads us to conclude that Fe-rich filaments testify to the recharge of deep magma a few days before high-energy explosive events, even when primitive magmas are not erupted.

Author Contributions

The co-authors contributed to the manuscript in the following ways: CD and CPM conceived and coordinated the writing and organization of the manuscript and figures; CD and PL collected samples at Stromboli; CD and PDC performed EMPA chemical mapping at University of Cambridge; CD and SCos performed textural analyses of ash and lapilli samples at SEM-EDS INGV-Pisa; CD, CPM, SCol and FB conceived the CFD simulations and FB performed the numerical simulations; SCol performed diffusion modelling; DM, AM and FA contributed to the final revision of the manuscript. All authors participated in the interpretation of results and finalization of the manuscript.

Acknowledgements

This work has benefited of the INGV Strategic Departmental Project UNO, for which we thank D. Andronico and A. Pontesilli for the support during sample collection at Stromboli; the INGV Departmental Project FIRST; and the INGV Pianeta Dinamico project DYNAMO. S. Costa was supported by MUR, PNRR project IR0000025 "Monitoring Earth's Evolution and Tectonics" MEET. We would like to thank the editor, Dr. Fabian Wadsworth, and the two reviewers, Dr. Dork Sahagian and Dr. Diego González García, whose comments and suggestions greatly improved the quality of the manuscript. The EMPA analyses were carried out at the University of Cambridge by I. Buisman, as part of the TNA-EXCITE project, and by M. Nazzari at the HP-HT INGV lab.

Data Availability

The software used for the diffusion modelling is available on Zenodo at https://doi.org/10.5281/zenodo.14610449. The setup for the numerical simulations of filament detachment is available as Supplementary Material 4 (solidLiquidMixing-D' Oriano2025 zip file).

References

Aiuppa, A., M. Bitetto, D. Delle Donne, F. P. La Monica, G. Tamburello, D. Coppola, M. Della Schiava, L. Innocenti, G. Lacanna, M. Laiolo, F. Massimetti, M. Pistolesi, M. C. Silengo, and M. Ripepe (2021). "Volcanic CO_2 tracks the incubation period of basaltic paroxysms". *Science Advances* 7(38). DOI: 10.1126/sciadv.abh0191.

Aiuppa, A., M. Bitetto, V. Francofonte, G. Velasquez, C. B. Parra, G. Giudice, M. Liuzzo, R. Moretti, Y. Moussallam, N. Peters, G. Tamburello, O. A. Valderrama, and A. Curtis (2017). "A CO_2-gas precursor to the March 2015 Villarrica volcano eruption". *Geochemistry, Geophysics, Geosystems* 18(6), pages 2120–2132. DOI: 10.1002/2017gc006892.

Alletti, M., D. R. Baker, and C. Freda (2007). "Halogen diffusion in a basaltic melt". *Geochimica et Cosmochimica Acta* 71(14), pages 3570–3580. DOI: 10.1016/j.gca.2007.04.018.

Andronico, D., C. D'Oriano, F. Pardini, A. La Spina, M. d. M. Vitturi, P. Bonfanti, A. Cristaldi, and F. Ferrari (2024). "The 23–24 March 2021 lava fountain at Mt Etna, Italy". *Bulletin of Volcanology* 86(6). DOI: 10.1007/s00445-024-01745-5.

Andronico, D., E. Del Bello, C. D'Oriano, P. Landi, F. Pardini, P. Scarlato, M. de'Michieli Vitturi, J. Taddeucci, A. Cristaldi, F. Ciancitto, F. Pennacchia, T. Ricci, and F. Valentini (2021). "Uncovering the eruptive patterns of the 2019 double paroxysm eruption crisis of Stromboli volcano". *Nature Communications* 12(1). DOI: 10.1038/s41467-021-24420-1.

Arzilli, F., C. Agostini, P. Landi, A. Fortunati, L. Mancini, and M. R. Carroll (2015). "Plagioclase nucleation and growth kinetics in a hydrous basaltic melt by decompression experiments". *Contributions to Mineralogy and Petrology* 170(5–6). DOI: 10.1007/s00410-015-1205-9.

Bellman, R. and R. H. Pennington (1954). "Effects of surface tension and viscosity on Taylor instability". *Quarterly of Applied Mathematics* 12(2), pages 151–162.

Bertagnini, A., N. Métrich, P. Landi, and M. Rosi (2003). "Stromboli volcano (Aeolian Archipelago, Italy): An open window on the deep-feeding system of a steady state basaltic volcano". *Journal of Geophysical Research: Solid Earth* 108(B7). DOI: 10.1029/2002jb002146.

Bertagnini, A., N. Méltrich, L. Francalanci, P. Landi, S. Tommasini, and S. Conticelli (2008). "Volcanology and Magma Geochemistry of the Present-Day Activity: Constraints on the Feeding System". *The Stromboli Volcano: An Integrated Study of the 2002-2003 Eruption*. Edited by S. Calvari, S. Inguaggiato, G. Puglisi, M. Ripepe, and M. Rosi. Volume 182. American Geophysical Union, pages 19–37. DOI: 10.1029/182gm04.

Bevilacqua, A., A. Bertagnini, M. Pompilio, P. Landi, P. Del Carlo, A. Di Roberto, W. Aspinall, and A. Neri (2020). "Major explosions and paroxysms at Stromboli (Italy): a new historical catalog and temporal models of occurrence with uncertainty quantification". *Scientific Reports* 10(1). DOI: 10.1038/s41598-020-74301-8.

Brogi, F., S. Colucci, J. Matrone, C. P. Montagna, M. De' Michieli Vitturi, and P. Papale (2022). "MagmaFOAM-1.0: a modular framework for the simulation of magmatic systems". *Geoscientific Model Development* 15(9), pages 3773–3796. DOI: 10.5194/gmd-15-3773-2022.

Cáceres, F., F. B. Wadsworth, B. Scheu, M. Colombier, C. Madonna, C. Cimarelli, K.-U. Hess, M. Kaliwoda, B. Ruthensteiner, and D. B. Dingwell (2020). "Can nanolites enhance eruption explosivity?" *Geology* 48(10), pages 997–1001. DOI: 10.1130/g47317.1.

Cahn, J. W. (1961). "On spinodal decomposition". *Acta Metallurgica* 9(9), pages 795–801. DOI: 10.1016/0001-6160(61)90182-1.

Caricchi, L., C. P. Montagna, A. Aiuppa, J. Lages, G. Tamburello, and P. Papale (2024). "CO2 Flushing Triggers Paroxysmal Eruptions at Open Conduit Basaltic Volcanoes". *Journal of Geophysical Research: Solid Earth* 129(4). DOI: 10.1029/2023jb028486.

Charlier, B. and T. L. Grove (2012). "Experiments on liquid immiscibility along tholeiitic liquid lines of descent". *Contributions to Mineralogy and Petrology* 164(1), pages 27–44. DOI: 10.1007/s00410-012-0723-y.

Colucci, S. (2025). "Multicomponent diffusion model". *Zenodo*. DOI: 10.5281/ZENODO.14610449. [Software].

Colucci, S., F. Brogi, G. Sottili, C. P. Montagna, and P. Papale (2024). "Short-term magma-carbonate interaction: A modelling perspective". *Earth and Planetary Science Letters* 628, page 118592. DOI: 10.1016/j.epsl.2024.118592.

D'Oriano, C., P. Del Carlo, D. Andronico, R. Cioni, P. Gabellini, A. Cristaldi, and M. Pompilio (2022). "Syn-Eruptive Processes During the January–February 2019 Ash-Rich Emissions Cycle at Mt. Etna (Italy): Implications for Petrological Monitoring of Volcanic Ash". *Frontiers in Earth Science* 10. DOI: 10.3389/feart.2022.824872.

Di Carlo, I. (2006). "Experimental Crystallization of a High-K Arc Basalt: the Golden Pumice, Stromboli Volcano (Italy)". *Journal of Petrology* 47(7), pages 1317–1343. DOI: 10.1093/petrology/egl011.

Di Fiore, F., A. Vona, D. Di Genova, A. Pontesilli, L. Calabrò, S. Mollo, J. Taddeucci, C. Romano, and P. Scarlato (2024). "Magma titanium and iron contents dictate crystallization timescales and rheological behaviour in basaltic volcanic systems". *Communications Earth & Environment* 5(1). DOI: 10.1038/s43247-024-01452-1.

Di Genova, D., R. A. Brooker, H. M. Mader, J. W. E. Drewitt, A. Longo, J. Deubener, D. R. Neuville, S. Fanara, O. Shebanova, S. Anzellini, F. Arzilli, E. C. Bamber, L. Hennet, G. La Spina, and N. Miyajima (2020). "In situ observation of nanolite growth in volcanic melt: A driving force for explosive eruptions". *Science Advances* 6(39). DOI: 10.1126/sciadv.abb0413.

Garg, D. and P. Papale (2022). "High-Performance Computing of 3D Magma Dynamics, and Comparison With 2D Simulation Results". *Frontiers in Earth Science* 9. DOI: 10.3389/feart.2021.760773.

Giordano, D., J. K. Russell, and D. B. Dingwell (2008). "Viscosity of magmatic liquids: A model". *Earth and Planetary*

Science Letters 271(1–4), pages 123–134. DOI: 10.1016/j.epsl.2008.03.038.

González-García, D., T. Boulesteix, A. Klügel, and F. Holtz (2023). "Bubble-enhanced basanite–tephrite mixing in the early stages of the Cumbre Vieja 2021 eruption, La Palma, Canary Islands". *Scientific Reports* 13(1). DOI: 10.1038/s41598-023-41595-3.

Grove, T. L. and M. B. Baker (1984). "Phase equilibrium controls on the tholeiitic versus calc-alkaline differentiation trends". *Journal of Geophysical Research: Solid Earth* 89(B5), pages 3253–3274. DOI: 10.1029/jb089ib05p03253.

Grove, T. L., R. J. Kinzler, and W. B. Bryan (1992). "Fractionation of Mid-Ocean Ridge Basalt (MORB)". *Mantle Flow and Melt Generation at Mid-Ocean Ridges*. Edited by J. P. Morgan, D. K. Blackman, and J. M. Sinton. American Geophysical Union, pages 281–310. ISBN: 9780875900353. DOI: 10.1029/gm071p0281.

Guo, C. and Y. Zhang (2020). "Multicomponent diffusion in a basaltic melt: Temperature dependence". *Chemical Geology* 549, page 119700. DOI: 10.1016/j.chemgeo.2020.119700.

Honour, V. C., M. B. Holness, B. Charlier, S. C. Piazolo, O. Namur, T. J. Prosa, I. Martin, R. T. Helz, J. Maclennan, and M. M. Jean (2019a). "Compositional boundary layers trigger liquid unmixing in a basaltic crystal mush". *Nature Communications* 10(1). DOI: 10.1038/s41467-019-12694-5.

Honour, V. C., M. B. Holness, J. L. Partridge, and B. Charlier (2019b). "Microstructural evolution of silicate immiscible liquids in ferrobasalts". *Contributions to Mineralogy and Petrology* 174(9). DOI: 10.1007/s00410-019-1610-6.

Honour, V. C. (2020). "Microstructural evolution of silicate immiscible liquids in solidifying ferrobasalts". PhD thesis. University of Cambridge. DOI: 10.17863/CAM.50738.

Hornby, A. J., P. M. Ayris, D. E. Damby, S. Diplas, J. Eychenne, J. E. Kendrick, C. Cimarelli, U. Kueppers, B. Scheu, J. E. P. Utley, and D. B. Dingwell (2024). "Nanoscale silicate melt textures determine volcanic ash surface chemistry". *Nature Communications* 15(1). DOI: 10.1038/s41467-024-44712-6.

Jollands, M. C. (2020). "Assessing analytical convolution effects in diffusion studies: Applications to experimental and natural diffusion profiles". *PLOS ONE* 15(11). Edited by M. Lepidi, e0241788. DOI: 10.1371/journal.pone.0241788.

Knafelc, J., S. E. Bryan, M. W. M. Jones, D. Gust, G. Mallmann, H. E. Cathey, A. J. Berry, E. C. Ferré, and D. L. Howard (2022). "Havre 2012 pink pumice is evidence of a short-lived, deep-sea, magnetite nanolite-driven explosive eruption". *Communications Earth & Environment* 3(1). DOI: 10.1038/s43247-022-00355-3.

La Felice, S. and P. Landi (2011). "The 2009 paroxysmal explosions at Stromboli (Italy): magma mixing and eruption dynamics". *Bulletin of Volcanology* 73(9), pages 1147–1154. DOI: 10.1007/s00445-011-0502-z.

La Spina, G., M. Burton, M. de'Michieli Vitturi, and F. Arzilli (2016). "Role of syn-eruptive plagioclase disequilibrium crystallization in basaltic magma ascent dynamics". *Nature Communications* 7(1). DOI: 10.1038/ncomms13402.

Laiolo, M., M. Ripepe, C. Cigolini, D. Coppola, M. Della Schiava, R. Genco, L. Innocenti, G. Lacanna, E. Marchetti, F. Massimetti, and M. C. Silengo (2019). "Space- and Ground-Based Geophysical Data Tracking of Magma Migration in Shallow Feeding System of Mount Etna Volcano". *Remote Sensing* 11(10), page 1182. DOI: 10.3390/rs11101182.

Landi, P., C. D'Oriano, M. Petrelli, M. Nazzari, and D. Andronico (2022). "Inferences on the magmatic plumbing system at Stromboli volcano (Italy) from trace element geochemistry of matrix glasses and minerals in different types of explosive eruptions". *Contributions to Mineralogy and Petrology* 177(10). DOI: 10.1007/s00410-022-01962-1.

Landi, P., N. Métrich, A. Bertagnini, and M. Rosi (2004). "Dynamics of magma mixing and degassing recorded in plagioclase at Stromboli (Aeolian Archipelago, Italy)". *Contributions to Mineralogy and Petrology* 147(2), pages 213–227. DOI: 10.1007/s00410-004-0555-5.

Lange, R. A. and I. S. E. Carmichael (1987). "Densities of Na2O-K2O-CaO-MgO-FeO-Fe2O3-Al2O3-TiO2-SiO2 liquids: New measurements and derived partial molar properties". *Geochimica et Cosmochimica Acta* 51(11), pages 2931–2946. DOI: 10.1016/0016-7037(87)90368-1.

Laumonier, M., B. Scaillet, L. Arbaret, and R. Champallier (2014). "Experimental simulation of magma mixing at high pressure". *Lithos* 196–197, pages 281–300. DOI: 10.1016/j.lithos.2014.02.016.

Le Gall, N. and M. Pichavant (2016). "Experimental simulation of bubble nucleation and magma ascent in basaltic systems: Implications for Stromboli volcano". *American Mineralogist* 101(9), pages 1967–1985. DOI: 10.2138/am-2016-5639.

Lormand, C., G. F. Zellmer, N. Sakamoto, T. Ubide, G. Kilgour, H. Yurimoto, A. Palmer, K. Németh, Y. Iizuka, and A. Moebis (2021). "Shallow magmatic processes revealed by cryptic microantecrysts: a case study from the Taupo Volcanic Zone". *Contributions to Mineralogy and Petrology* 176(11). DOI: 10.1007/s00410-021-01857-7.

Métrich, N., A. Bertagnini, P. Landi, and M. Rosi (2001). "Crystallization Driven by Decompression and Water Loss at Stromboli Volcano (Aeolian Islands, Italy)". *Journal of Petrology* 42(8), pages 1471–1490. DOI: 10.1093/petrology/42.8.1471.

Métrich, N., A. Bertagnini, and M. Pistolesi (2021). "Paroxysms at Stromboli Volcano (Italy): Source, Genesis and Dynamics". *Frontiers in Earth Science* 9. DOI: 10.3389/feart.2021.593339.

Mollo, S. and J. E. Hammer (2017). "Dynamic crystallization in magmas". *Mineral reaction kinetics: Microstructures, textures, chemical and isotopic signatures*. Edited by W. Heinrich and R. Abart. Volume 16. Mineralogical Society of Great Britain & Ireland, pages 378–418. ISBN: 9780903056649. DOI: 10.1180/emu-notes.16.12.

Morgavi, D., I. Arienzo, C. Montagna, D. Perugini, and D. B. Dingwell (2017). "Magma Mixing: History and Dynamics of an Eruption Trigger". *Volcanic Unrest*. Springer International Publishing, pages 123–137. ISBN: 9783319584126. DOI: 10.1007/11157_2017_30.

Neave, D. A., P. Beckmann, H. Behrens, and F. Holtz (2021). "Mixing between chemically variable primitive basalts cre-

ates and modifies crystal cargoes". *Nature Communications* 12(1). DOI: 10.1038/s41467-021-25820-z.

Petrone, C. M., S. Mollo, R. Gertisser, Y. Buret, P. Scarlato, E. Del Bello, D. Andronico, B. Ellis, A. Pontesilli, G. De Astis, P. P. Giacomoni, M. Coltorti, and M. Reagan (2022). "Magma recharge and mush rejuvenation drive paroxysmal activity at Stromboli volcano". *Nature Communications* 13(1). DOI: 10.1038/s41467-022-35405-z.

Pichavant, M., I. Di Carlo, M. Pompilio, and N. Le Gall (2022). "Timescales and mechanisms of paroxysm initiation at Stromboli volcano, Aeolian Islands, Italy". *Bulletin of Volcanology* 84(4). DOI: 10.1007/s00445-022-01545-9.

Pioli, L., M. Pistolesi, and M. Rosi (2014). "Transient explosions at open-vent volcanoes: The case of Stromboli (Italy)". *Geology* 42(10), pages 863–866. DOI: 10.1130/g35844.1.

Ripepe, M., G. Lacanna, M. Pistolesi, M. C. Silengo, A. Aiuppa, M. Laiolo, F. Massimetti, L. Innocenti, M. Della Schiava, M. Bitetto, F. P. La Monica, T. Nishimura, M. Rosi, D. Mangione, A. Ricciardi, R. Genco, D. Coppola, E. Marchetti, and D. Delle Donne (2021). "Ground deformation reveals the scale-invariant conduit dynamics driving explosive basaltic eruptions". *Nature Communications* 12(1). DOI: 10.1038/s41467-021-21722-2.

Romero, J. E., E. Morgado, A. Pisello, F. Boschetty, M. Petrelli, F. Cáceres, M. A. Alam, M. Polacci, J. L. Palma, F. Arzilli, F. Vera, R. Gutiérrez, and D. Morgavi (2022). "Pre-eruptive Conditions of the 3 March 2015 Lava Fountain of Villarrica Volcano (Southern Andes)". *Bulletin of Volcanology* 85(1). DOI: 10.1007/s00445-022-01621-0.

Rosi, M., M. Pistolesi, A. Bertagnini, P. Landi, M. Pompilio, and A. Di Roberto (2013). "Chapter 14 Stromboli volcano, Aeolian Islands (Italy): present eruptive activity and hazards". *Geological Society, London, Memoirs* 37(1), pages 473–490. DOI: 10.1144/m37.14.

Shea, T. and J. E. Hammer (2013). "Kinetics of cooling- and decompression-induced crystallization in hydrous mafic-intermediate magmas". *Journal of Volcanology and Geothermal Research* 260, pages 127–145. DOI: 10.1016/j.jvolgeores.2013.04.018.

Taddeucci, J., C. Cimarelli, M. A. Alatorre-Ibargüengoitia, H. Delgado-Granados, D. Andronico, E. Del Bello, P. Scarlato, and F. Di Stefano (2021). "Fracturing and healing of basaltic magmas during explosive volcanic eruptions". *Nature Geoscience* 14(4), pages 248–254. DOI: 10.1038/s41561-021-00708-1.

Valdivia, P., A. Zandoná, A. Kurnosov, T. B. Ballaran, J. Deubener, and D. Di Genova (2023). "Are volcanic melts less viscous than we thought? The case of Stromboli basalt". *Contributions to Mineralogy and Petrology* 178(7). DOI: 10.1007/s00410-023-02024-w.

Veksler, I. V. and B. Charlier (2015). "Silicate Liquid Immiscibility in Layered Intrusions". *Layered Intrusions*. Edited by B. Charlier, O. Namur, R. Latypov, and C. Tegner. Springer Netherlands, pages 229–258. ISBN: 9789401796521. DOI: 10.1007/978-94-017-9652-1_5.

Vergniolle, S. and N. Métrich (2022). "An interpretative view of open-vent volcanoes". *Bulletin of Volcanology* 84(9). DOI: 10.1007/s00445-022-01581-5.

Villiger, S., P. Ulmer, and O. Müntener (2006). "Equilibrium and Fractional Crystallization Experiments at 0middle dot7 GPa; the Effect of Pressure on Phase Relations and Liquid Compositions of Tholeiitic Magmas". *Journal of Petrology* 48(1), pages 159–184. DOI: 10.1093/petrology/egl058.

Villiger, S., P. Ulmer, O. Müntener, and A. B. Thompson (2004). "The Liquid Line of Descent of Anhydrous, Mantle-Derived, Tholeiitic Liquids by Fractional and Equilibrium Crystallization–an Experimental Study at 1.0 GPa". *Journal of Petrology* 45(12), pages 2369–2388. DOI: 10.1093/petrology/egh042.

Voloschina, M., N. Métrich, A. Bertagnini, P. Marianelli, A. Aiuppa, M. Ripepe, and M. Pistolesi (2023). "Explosive eruptions at Stromboli volcano (Italy): a comprehensive geochemical view on magma sources and intensity range". *Bulletin of Volcanology* 85(6). DOI: 10.1007/s00445-023-01647-y.

Wadsworth, F. B., E. W. Llewellin, J. I. Farquharson, J. K. Gillies, A. Loisel, L. Frey, E. Ilyinskaya, T. Thordarson, S. Tramontano, E. Lev, M. J. Pankhurst, A. G. Rull, M. Asensio-Ramos, N. M. Pérez, P. A. Hernández, D. Calvo, M. C. Solana, U. Kueppers, and A. P. Santabárbara (2022). "Crowd-sourcing observations of volcanic eruptions during the 2021 Fagradalsfjall and Cumbre Vieja events". *Nature Communications* 13(1). DOI: 10.1038/s41467-022-30333-4.

Wiesmaier, S., D. Morgavi, C. J. Renggli, D. Perugini, C. P. De Campos, K.-U. Hess, W. Ertel-Ingrisch, Y. Lavallée, and D. B. Dingwell (2015). "Magma mixing enhanced by bubble segregation". *Solid Earth* 6(3), pages 1007–1023. DOI: 10.5194/se-6-1007-2015.

Yoshida, K., A. Miyake, S. H. Okumura, H. Ishibashi, S. Okumura, A. Okamoto, Y. Niwa, M. Kimura, T. Sato, Y. Tamura, and S. Ono (2023). "Oxidation-induced nanolite crystallization triggered the 2021 eruption of Fukutoku-Oka-no-Ba, Japan". *Scientific Reports* 13(1). DOI: 10.1038/s41598-023-34301-w.

Yoshimura, S., T. Kuritani, A. Matsumoto, and M. Nakagawa (2019). "Fingerprint of silicic magma degassing visualised through chlorine microscopy". *Scientific Reports* 9(1). DOI: 10.1038/s41598-018-37374-0.

Zellmer, G. F., N. Sakamoto, S.-L. Hwang, N. Matsuda, Y. Iizuka, A. Moebis, and H. Yurimoto (2016). "Inferring the Effects of Compositional Boundary Layers on Crystal Nucleation, Growth Textures, and Mineral Chemistry in Natural Volcanic Tephras through Submicron-Resolution Imaging". *Frontiers in Earth Science* 4. DOI: 10.3389/feart.2016.00088.

Zhang, Y. and T. Gan (2022). "Diffusion in Melts and Magmas". *Reviews in Mineralogy and Geochemistry* 87(1), pages 283–337. DOI: 10.2138/rmg.2022.87.07.